# High-Bandwidth Organic Light Emitting Diodes for Ultra-Low Cost Visible Light Communication Links

**Priyanka de Souza[a], Nikos Bamiedakis[a], Kou Yoshida[b], Pavlos P. Manousiadis[b], Graham A. Turnbull[b], Ifor D. W. Samuel[b], Richard V. Penty[a] and Ian H. White[a]**

[a] *Electrical Engineering Division, Department of Engineering, University of Cambridge, 9 JJ Thomson Avenue, Cambridge CB3 0FA, UK*

[b] *Organic Semiconductor Centre, SUPA, School of Physics and Astronomy, University of St. Andrews, St. Andrews KY16 9SS, UK*

*e-mail: ped24@cam.ac.uk*

## ABSTRACT

Visible light communications (VLC) have attracted considerable interest in recent years due to an increasing need for data communication links in home and enterprise environments. Organic light-emitting diodes (OLEDs) are widely used in display applications owing to their high brightness, high quality colour-rending capability and low cost. As a result, they are attractive candidates for the implementation of ultra-low cost visible light optical links in free-space and guided-wave communications. However, OLEDs need to exhibit a bandwidth of at least ~MHz to be able to support the modest data rates (~Mbps) required in these applications. Although fluorescent OLEDs typically exhibit shorter photon lifetimes than inorganic LEDs, the bandwidth performance of the large size OLEDs used in display applications are limited by their electrical characteristics. In this work, we present a detailed physical simulation that describes well the performance of fast OLED devices that exhibit significant -3 dB bandwidths ($f_{-3dB}$) of 44 MHz obtained for a 0.12 $mm^2$ device. It is demonstrated that the reduction of the device size results in a significant bandwidth improvement due primarily to a reduction in parasitic capacitance of the devices, though this is counteracted by carrier dynamic effects. The model provides an insight into the basic physical properties of the OLED and may be used for optimisation of future generations of OLED devices.

**Keywords**: OLED, simulation, modelling, visible light communications.

## 1. INTRODUCTION

In an era of ever-increasing data generation and transmission, visible light communications (VLC) has attracted significant interest for end-user applications. Organic LEDs (OLEDs) can be deposited using a variety of technologies on a multitude of different substrates. They show high brightness and have a relatively low cost, making them good candidates for low-cost VLC links [1], particularly as advanced coding and array techniques may eventually enable >Gbps aggregate data rates [2]. However, the inherently low mobility of organic semiconductors means that they are often bandwidth-limited and can struggle to achieve the ~Mbps data rates required (at a minimum) for use in communications. Nonetheless, with analysis and optimisation afforded by simulation and modelling techniques, it may be possible to understand better the behaviour of such organic devices and correspondingly to optimise their design for such high-bandwidth applications.

In this work, we present the physical modelling and characterisation of a multi-stack OLED with the aim of optimising the devices for communications purposes. To the best of the authors' knowledge, this is the first demonstration of an experimentally-validated five-layer OLED simulation fitting both DC current-voltage and small signal characteristics. Previous simulations have been used to model OLEDs, but have focussed on simpler single- or double-layer devices [3]–[6] or have not considered small signal characteristics [7]. In this paper, we bring together both the dynamic and static characteristics for an holistic device simulation. We see that the devices are significantly RC limited, and by scaling down in device dimensions we accordingly see an increase in predicted bandwidth from 8 MHz for the 9 $mm^2$ devices, to 50 MHz for the 0.12 $mm^2$ devices.

## 2. OLEDs

The OLEDs presented in this paper are manufactured using thermal evaporation on glass substrates, with epoxy and 1 mm thick glass used to encapsulate the devices. The five-layer top-emitting OLED stack (F1A) can be seen in Fig. 1(a), with thin silver used as a semi-transparent cathode, and aluminium as the cathode. The materials used in the OLED stack are 4,7-diphenyl-1,10-phenanthroline (BPhen) doped with 2wt% caesium as an electron injection layer, bis-(2-methyl-8-chinolinolato)-(4-phenyl-phenolato)-aluminium(III) (BAlq) as a hole blocking layer, 2-methyl-9,10-di(2-naphthyl)anthracene (MADN) doped with 2.76wt% 2,5,8,11-tetra-tert-butylperylene (TBPe) as the emissive layer, N,N'-di(naphthalene-1-yl)-N-N'-diphenylbenzidiene (α-NPD) as the electron blocking layer and 2,2',7,7'-tetrakis(N,N'-di-p-methylphenylamino)-9,9'-spirobifluorene (Spiro-TTB) doped with 4wt% 2,2'-(perfluoronaphthalene-2,6-diylidene)dimalononitrile ($F_6$-TCNNQ) as the hole injection layer, with layer thicknesses as shown in Fig. 1. A 40nm α-NPD capping layer is evaporated on the thin silver to enhance the out-coupling of emitted light to the air; this is ignored in this study for simplicity as it is believed it has no

effect upon the electrical properties. The devices have been fabricated with three different area dimensions: 0.3×0.4 $mm^2$ (S), 1×1.1 $mm^2$ (M) and 3×3 $mm^2$ (L) in order to study their bandwidth performance as a function of device size. Two four-layer devices are also fabricated to use as control samples for model validation; these devices are missing either the Spiro-TTB layer [SP3A, Fig. 1(b)] or the BPhen layer [BP1D, Fig. 1(c)], which act respectively as the electron and hole injection layer.

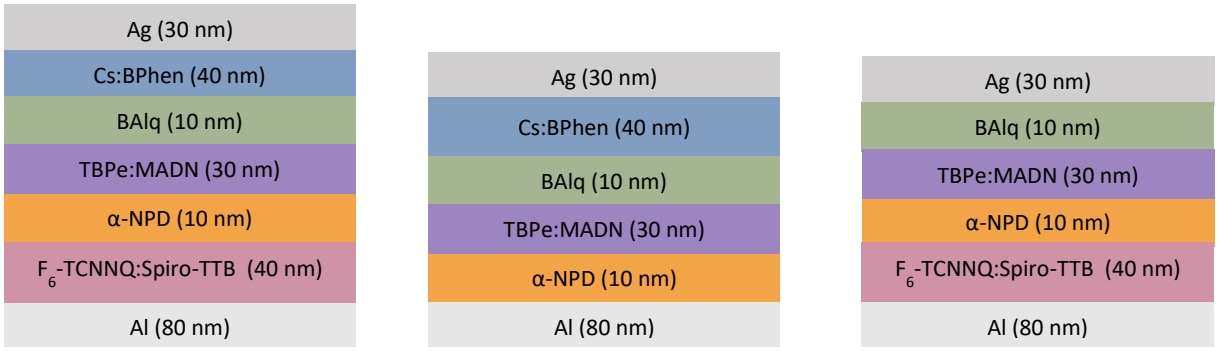


*Fig. 1:(a) Full OLED stack (F1A), (b) OLED without Spiro-TTB (SP3A), (c) OLED without BPhen (BP1D)*

## 3. SIMULATION

### 3.1 Device physics

The simulation of the devices is undertaken in commercially available Silvaco ATLAS software. The software solves Poisson's equation and the continuity and constitutive equations to determine the electrical performance of semiconductor devices. By including Langevin recombination parameters and exciton generation and recombination parameters, it is also possible to extract the optical power.

The highest occupied molecular orbital (HOMO), and lowest unoccupied molecular orbital (LUMO), analogous to the valence band and conduction band for each material, are set by specifying electron affinity and band gap parameters. The organic materials are simulated as having Gaussian band structures, with carrier densities in the HOMO and LUMO then evaluated numerically using Fermi-Dirac statistics. For these OLEDs, a Poole-Frenkel field-dependent mobility model is used, according to equation (1).

$$\mu_{n_{PF}}(E) = \mu_{n0}\, exp\left(\sqrt{\frac{|\boldsymbol{E}|}{E_{0n_{PF}}}} - \gamma_{n_{PF}}\sqrt{|\boldsymbol{E}|}\right) \tag{1}$$

where $\mu_{n0}$is the zero-field mobility, $E_{0n_{PF}}$ is the characteristic field, **E** is the Electric field and $\gamma_{n_{PF}}$ describes the field-dependent mobility factor. Carrier recombination is modelled using a Langevin recombination rate:

$$R_{Ln,p} = \frac{q\left[\mu_n(E) + \mu_p(E)\right]}{\varepsilon_r \varepsilon_0}(np - n_i^2) \tag{2}$$

The doped layers are simulated by the addition of a uniform carrier concentration of charge throughout the relevant layers. Carrier injection at organic interfaces and at the contacts is modelled as thermionic emission, and a fixed defect density with a band-like distribution of defects is assumed within the layers. A 2.5 Ω resistance is modelled at each contact, with the workfunctions of the metal contacts modified depending upon the organic material the contact is deposited onto; this is based upon the widely-reported workfunction-lowering phenomenon at metal-organic interfaces [8]–[11].

The simulation parameters given in Table 1 are based upon literature values and experimental curve fitting where appropriate parameters could not be found. Where unknown, the density of states used is calculated using an approximate molecular density, and, in the case of dopants, assumes a doping efficiency of the order of a few percent, in accordance with the literature [12].

*Table 1: Significant simulation parameters*

| | **Spiro-TTB** | **α-NPD** | **MADN** | **BAlq** | **BPhen** |
|---|---|---|---|---|---|
| $\boldsymbol{E_C}$ **(eV) /** $\boldsymbol{E_V}$ **(eV)** | 2.7 / 6.0 | 2.4 / 5.7 | 3.0 / 5.6 | 2.7 / 6.1 | 2.4 / 6.0 |
| $\boldsymbol{N_C, N_V}$ **(cm$^{-3}$)** | $8.2\times10^{20}$ | $1.24\times10^{21}$ | $1.6\times10^{21}$ | $3\times10^{21}$ | $2.19\times10^{21}$ |
| $\boldsymbol{\sigma_C, \sigma_V}$ **(eV)** | 0.2 | 0.22 | 0.2 | 0.15 | 0.08 |
| $\boldsymbol{\mu_{n/p0}}$ **(cm$^2$/Vs)** | $4\times10^{-7}$ | $6.3\times10^{-6}$ | $1\times10^{-6}$ | $5\times10^{-7}$ | $5.5\times10^{-5}$ |
| $\boldsymbol{\gamma_{n/p_{PF}}}$ **(cm/V)$^{0.5}$** | $-4\times10^{-3}$ | $-4\times10^{-3}$ | $-8\times10^{-3}$ | $-7\times10^{-3}$ | $-8\times10^{-4}$ |
| | **$F_6$TCNNQ** | | **TBPe** | | **Cs** |
| **Doping (cm$^{-3}$)** | $1.4\times10^{18}$ | | $1.8\times10^{17}$ | | $2\times10^{18}$ |

## 4. RESULTS

### 4.1 Device Measurement & Simulation Results

The current-voltage (I-V) and light-voltage (L-V) characteristics of the devices are obtained using an optical lens and a broad-area detector. The I-V and L-V characteristics of the respective OLEDs are also obtained from the simulation model and shown in Fig. 2 and Fig. 4 for comparison. As the light output power obtained from the simulation does not include any external coupling losses, the output power values for all devices are normalised to the maximum power measured from the full stack device. A reasonable fit is obtained between the simulation and experimental results for both curves and all types of devices. The emission spectrum for each type of device is also recorded and shown in Fig. 3.

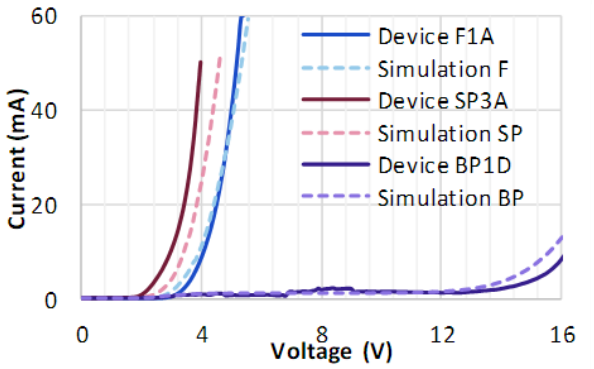


*Fig. 2: Measured (solid) and simulated (dashed) I-V curves for the devices under test*

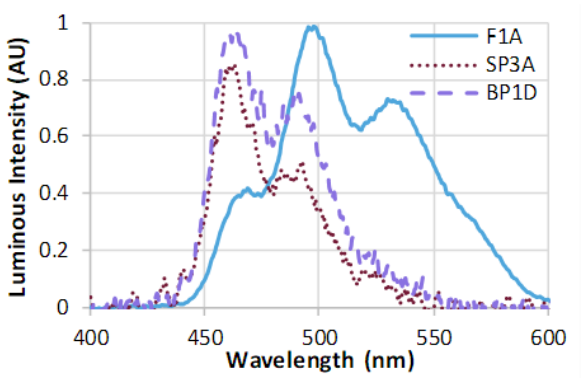


*Fig. 3: Measured electroluminescence spectra of the devices*

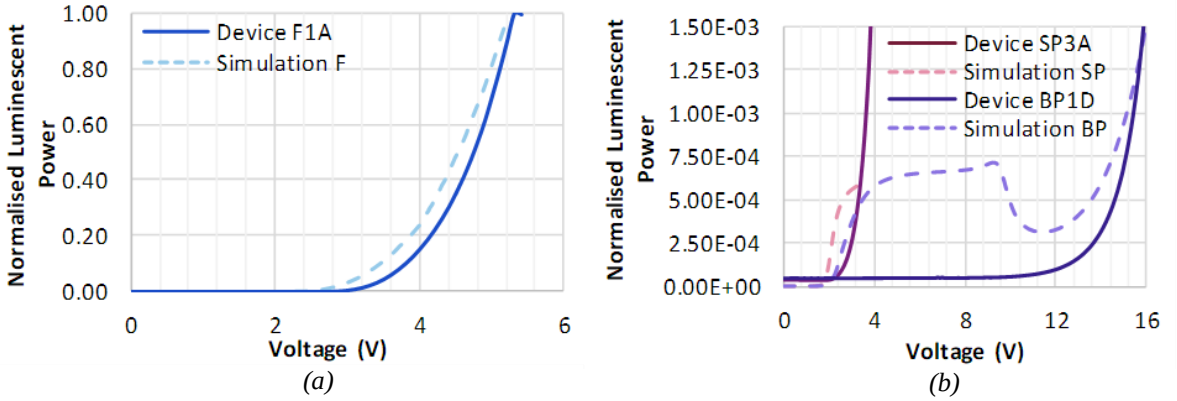


*(a)* *(b)*

*Fig. 4: Simulation (dashed) and measurement (solid) light-voltage curves for (a) the full stack devices and for (b) the devices without Spiro-TTB (SP3A) and without BPhen (BP1D)*

The devices that exclude the hole injection and electron injection layers show very low luminescent power output, indicating that they are electron-only (SP3A) and hole-only (BP1D) devices respectively. This is corroborated by the simulation, which shows very low luminescent power output in these predominantly single-carrier devices, with recombination no longer occurring in the MADN emissive layer, but in the $BAlq_3$ and α-NPD layers. This would also agree with the spectral shift in Fig. 3 measured between the full-stack devices and the single-carrier devices, which shows peaks corresponding to the electroluminescence peaks for $BAlq_3$/α-NPD devices [13]. The results confirm the importance of the presence of these two layers in the OLED stack for achieving efficient charge injection of both electrons and holes.

### 4.2 Bandwidth Measurements

The frequency response of the differently-sized full-stack OLEDs is measured using a vector network analyser (VNA, Keysight N9913A) at different bias currents. The light output from the RF-modulated OLED is fed to an 800 μm diameter avalanche photodiode (APD, First Sensor AD800-11) via a 1 mm diameter plastic optical fibre (POF) patch cord and a pair of optical lenses. The received electrical signal is amplified before being input into the VNA for $S_{21}$ measurements. The bandwidth of the photodiode and amplifier is ~650 MHz; this is much greater than that of the OLEDs, so the results from the VNA may be used to directly assess the bandwidth of the OLED.

Fig. 5 shows the experimentally-measured -3 dB bandwidths of the three different device sizes at various bias currents, with simulation bandwidths calculated from extracted small signal resistance and conductance values. It is found that the small, medium and large devices exhibit -3 dB bandwidths of up to 44, 15 and 3.8 MHz, respectively. It is observed that the model yields slightly larger bandwidth values at high currents; this is perhaps

due to a slightly high field-enhancement mobility factor. Nevertheless, the reduction in device area affords a great improvement in bandwidth as one would expect a reduction in device capacitance. However, the bandwidth does not scale inversely with the device area as expected, and so additional physical effects such as carrier transport and dynamics are likely to have an influence.

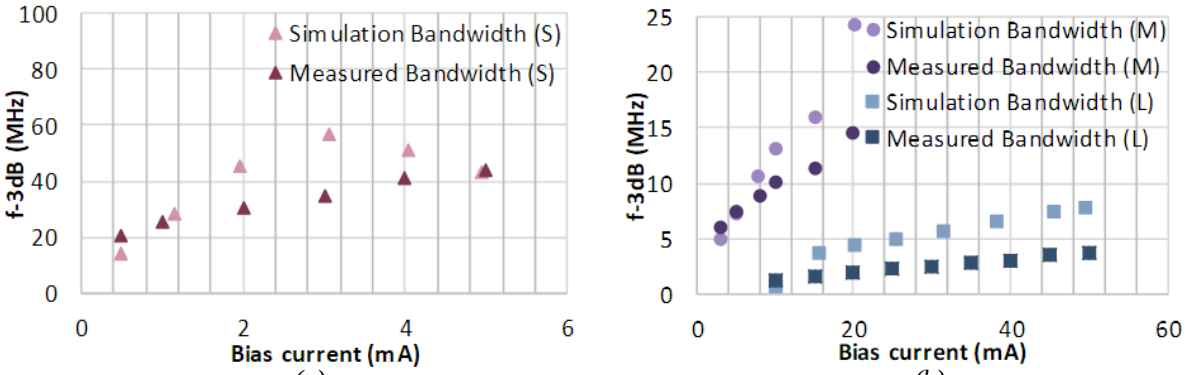


*(a)* *(b)*

*Fig. 5: -3 dB bandwidth measurements and simulation results at different DC bias currents for three OLED sizes: (a) 0.12 mm$^2$ (S) and (b) 1.1 mm$^2$ (M) & 9 mm$^2$ (L).*

## 5. CONCLUSIONS

OLEDs may be deployed in VLC links, provided they can support ~Mbps data transmission. Here, OLEDs emitting at 495 nm and exhibiting a -3 dB bandwidth of 44 MHz are demonstrated. It is shown that the reduction of OLED size significantly improves the bandwidth performance. A detailed simulation model is produced that accurately predicts the DC and dynamic characteristics of the devices and that can be deployed for the optimisation of their high-speed performance.

## ACKNOWLEDGEMENTS

This work was supported by the UK EPSRC via the Ultra Parallel Visible Light Communication Project (EP/K00042X/1) and EPSRC Studentship 1466721. Additional data related to this publication is available at the data repository https://doi.org/10.17863/CAM.22394.

## REFERENCES

[1] P. A. Haigh, Z. Ghassemlooy, S. Rajbhandari, and I. Papakonstantinou, 'Visible light communications using organic light emitting diodes', *IEEE Commun. Mag.*, vol. 51, no. 8, pp. 148–154, Aug. 2013.

[2] L. Zeng *et al.*, 'High data rate multiple input multiple output (MIMO) optical wireless communications using white led lighting', *IEEE J. Sel. Areas Commun.*, vol. 27, no. 9, pp. 1654–1662, Dec. 2009.

[3] W. Zhou, C. Zimmermann, and C. Jungemann, 'Numerical Capacitance Analysis of Single-Layer OLEDs Based on the Master Equation', *IEEE Trans. Electron Devices*, vol. 63, no. 12, pp. 4919–4923, Dec. 2016.

[4] H. Siemund and H. Göbel, 'Numerical Simulation of Organic Light-Emitting Diodes With Insulating Cathode Buffer Layer', *IEEE Trans. Electron Devices*, vol. 63, no. 9, pp. 3700–3706, Sep. 2016.

[5] E. Knapp and B. Ruhstaller, 'Numerical analysis of steady-state and transient charge transport in organic semiconductor devices', *Opt. Quantum Electron.*, vol. 42, no. 11–13, pp. 667–677, Oct. 2011.

[6] N. D. Nguyen and M. Schmeits, 'Numerical simulation of impedance and admittance of OLEDs', *Phys. Status Solidi A*, vol. 203, no. 8, pp. 1885–1885, Jun. 2006.

[7] B. Ruhstaller *et al.*, '59.1: Invited Paper: Optoelectronic OLED Modeling for Device Optimization and Analysis', *SID Symp. Dig. Tech. Pap.*, vol. 38, no. 1, pp. 1686–1690, May 2007.

[8] B. Jaeckel, J. B. Sambur, and B. A. Parkinson, 'Ubiquitous Pentacene Monolayer on Metals Deposited onto Pentacene Films', *Langmuir*, vol. 23, no. 23, pp. 11366–11368, Nov. 2007.

[9] I. G. Hill, A. Rajagopal, and A. Kahn, 'Energy-level alignment at interfaces between metals and the organic semiconductor 4,4′-N,N′-dicarbazolyl-biphenyl', *J. Appl. Phys.*, vol. 84, no. 6, pp. 3236–3241, Sep. 1998.

[10] S. Olthof, R. Meerheim, M. Schober, and K. Leo, 'Energy level alignment at the interfaces in a multilayer organic light-emitting diode structure', *Phys. Rev. B*, vol. 79, no. 24, p. 245308, Jun. 2009.

[11] S. Braun, W. R. Salaneck, and M. Fahlman, 'Energy-Level Alignment at Organic/Metal and Organic/Organic Interfaces', *Adv. Mater.*, vol. 21, no. 14–15, pp. 1450–1472, Apr. 2009.

[12] Lüssem B., Riede M., and Leo K., 'Doping of organic semiconductors', *Phys. Status Solidi A*, vol. 210, no. 1, pp. 9–43, Dec. 2012.

[13] T. Mori and T. Itoh, 'EL Behavior for Blue-Emitting Aluminum Quinoline-Based Organic Light-Emitting Diodes', *J. Photopolym. Sci. Technol.*, vol. 22, no. 4, pp. 515–520, 2009.